DETERMINATION OF THE EFFECT OF VISCOELASTICITY ON THE BOND STRENGTH OF A DENTAL METAL-CERAMIC SYSTEM USING FINITE ELEMENT METHOD

by

Utku Cemal Ünlü

B.S., Mechanical Engineering, Boğaziçi University, 2004

Submitted to the Institute for Graduate Studies in
Science and Engineering in partial fulfillment of
the requirements for the degree of
Master of Science

Graduate Program in Mechanical Engineering
Boğaziçi University
2007

ACKNOWLEDGEMENTS

I would like to express my appreciation to Dr. Şebnem Özüpek for her helpful advice and guidance in all stages of this study. I feel lucky for being one of her students.

I would like to thank to my friends Hatice Mercan, Erhan Turan and Yalın Kaptan for their help and support.

Finally, I would like to thank to my parents Ayşe Ünlü, Remzi Ünlü, my sister Fatma Ünlü and my dear friend Yeliz Simitçioğlu for their love and moral support.

ABSTRACT

DETERMINATION OF THE EFFECT OF VISCOELASTICITY ON THE BOND STRENGTH OF A DENTAL METAL-CERAMIC SYSTEM USING FINITE ELEMENT METHOD

Porcelain-fused-to-metal (PFM) is a kind of restoration process used in prosthetic dentistry, where a certain metal is cast as basement on which the dental ceramic is fused by firing. Due to the difference in the coefficients of thermal expansion of the two materials, all PFM restorations contain thermal stresses, which develop during the cooling phase after firing. These thermal stresses coupled with the stresses produced by mechanical loads may be the dominant reasons for failures in clinical situations. For an accurate calculation of these stresses, viscoelastic behavior of ceramic at high temperatures should not be ignored.

In this study, the finite element technique is used to evaluate the effect of viscoelasticity on the bond strength of a three-point flexure test specimen, which is the current international standard, ISO 9693, to characterize the interfacial bond strength of metal-ceramic restorative systems. Although there are some studies which take into account the viscoelastic behavior of the ceramic in the determination of thermal stresses, none of them evaluates the effect of viscoelasticity on the bond strength, which is of great importance in assessing failure of PFM restorations. Evaluation of the results in the vicinity of the interface end, critical point for initial debonding, show that the load shear stress is offset by thermal residual stress, the normal stress is compressive for thermal load and tensile for mechanical load. This indicates that the probability of interfacial debonding due to normal tensile stress is higher than that due to shear stress.

ÖZET

VİSKOELASTİSİTENİN DENTAL METAL-SERAMİK BAĞ KUVVETİNE ETKİSİNİN SONLU ELEMANLAR METODU KULLANILARAK BELİRLENMESİ

Metal-Seramik kaplama, belli bir metalin üzerine dental seramiğin bir ısıl işlem sonucu kaynatılması ile oluşturulan bir diş protez restorasyon yöntemidir. Isıl işlem sırasında, iki malzemenin ısıl genleşme katsayılarındaki farklılık nedeni ile ısıl gerilmeler oluşur. Bu gerilmeler, mekanik yükleme sonucunda oluşan gerilmelerle birleştiğinde kırılmalara neden olabilmektedir. Isıl gerilmelerin tam olarak hesaplanabilmesi için seramiğin yüksek sıcaklıklarda gösterdiği viskoelastik davranış ihmal edilmemelidir.

Bu çalışmada, visckoelastisitenin metal-seramik protezlerde ara yüzeydeki bağ kuvvetini ölçmekte kullanılan şu anki uluslararası standart test olan ISO-9693 test numunesindeki ısıl gerilmelere etkisi sonlu elemanlar yöntemi kullanılarak hesaplanmıştır. Literatürde ısıl gerilmelerin hesaplanmasında viskoelastisitenin etkisini hesaba katan çalışmalar olduğu halde, bu çalışmaların hiçbirinde bağ kuvveti hesaplanmamıştır. Kopma noktası yakınlarındaki sonuçların değerlendirilmesi, mekanik kuvvetlerden doğan kayma gerilmelerinin ısıl artık gerilmeler tarafından kaydırıldığını, ısıl normal gerilmelerin basma ve mekanik normal gerilmelerin bükme yönünde olduğunu göstermiştir. Bu durum kopmanın kesme gerilmeleri yerine normal çekme gerilmelerinden kaynaklanması olasılığını artırmaktadır.

TABLE OF CONTENTS

LIST OF FIGURES

LIST OF TABLES

LIST OF SYMBOLS/ABBREVIATIONS

a_T	Shift values for viscoelastic material model
b	Width of the three-point bending specimen (DeHoff's model)
C	Creep rate
C_1, C_2	Constants of the WLF curve fit
d_c	Height of the ceramic part of the three-point bending specimen
d_m	Height of the metal part of the three-point bending specimen
E_M	Elastic Moduli of metal
E_C	Elastic Moduli of ceramic
F_fail	Failure load
F_x	Finite element internal nodal force output in X-direction
F_y	Finite element internal nodal force output in Y-direction
G	Relaxation function
G_1, G_2, G_3, G_4	Constants of the relaxation function
h	Height of the three-point bending specimen (DeHoff's model)
K	Bulk Modulus
K_0	Initial bulk modulus
L	Length of the three-point bending specimen (DeHoff's model)
l_c	Length of the ceramic part of the three-point bending specimen
P	Applied midpoint Load
S_{12}	Shear stress in xy plane
S_{22}	Normal stress in y direction
x^*	The point where the normal stress changes from tension to compression
α_C	Thermal expansion coefficient of ceramic
α_M	Thermal expansion coefficient of metal
η_s	Shear viscosity
ν_C	Poisson's ratio of ceramic

ν_M	Poisson's ratio of metal
σ_{xy}, σ_{12}	Shear stress in xy plane
σ_{yy}, σ_{22}	Normal stress in y direction
$\overline{\sigma}_{xy}, \overline{\sigma}_{12}$	Average shear stress
$\overline{\sigma}_{yy}, \overline{\sigma}_{22}$	Average normal stress
Θ_G	Glass transition temperature of ceramic
Θ_i	Initial temperature
Θ_R	Ambient temperature
$\tau_1, \tau_2, \tau_3, \tau_4$	Constants of the relaxation function

PFM	Porcelain Fused to Metal
ISO	International S
FEA	Finite Element Analysis
FE	Finite Elements
CPS4	4-node linear quadrilateral element
CPS8	8-node quadratic quadrilateral element
BBV	Beam Bending Viscometer
WLF	Williams-Landell-Ferry

1. INTRODUCTION

Metal-ceramic constructions used in dentistry combine high mechanical strength of metals with various advantageous features such as biocompatibility, high abrasion strength and unsurpassed aesthetic appearance of ceramics. They are stronger than all-ceramic constructions and their appearance is much more natural than all-metal constructions.

Metal and ceramic parts are joined together by using a technique called porcelain-fused-to-metal (PFM). PFM is a kind of restoration for teeth where a certain metal is cast as basement on which the dental ceramic is fused by firing. For the metal part, base alloys such as nickel base and cobalt base containing aluminum or titanium, semi-precious alloys (alloys of silver etc.) or precious alloys with high gold and platinum content can be used. Semi-precious alloys are stiffer and less expensive. However precious alloys are more malleable and therefore fit the tooth more accurately. Because of the difference in the coefficients of thermal expansion of the metal and porcelain, thermal stresses develop in all PFM restorations during the cooling after firing. The dominant reasons for failures in clinical situations are usually these thermal stresses coupled with stresses produced by mechanical load [1]. If the ceramic and the metal are properly bonded, failure occurs as brittle fracture or abrasive wear of the ceramic core, and not through the metal or at the ceramic-metal interface. Therefore, the success of metal-ceramic dental restorations depends greatly on the bond strength of the ceramic to the metal.

The standard procedure that is used today to characterize the bonding in metal-ceramic dental restorative systems is the three-point flexure test [2] proposed by Lenz et al [3]. In this test , the critical bending force is measured. This force is defined as the force under which debonding of the porcelain from the alloy strip occurs at one of the two ends of the ceramic layer.

In the study of Lenz *et al.* [3], finite element analysis of a three-point flexure specimen is performed and average stresses at the metal-ceramic interface are calculated. Bond strength of the specimen is defined in terms of the calculated average shear stress and measured critical bending force. The proposed method, which is a combination of experimental and numerical studies, is capable of distinguishing bond strengths of excellent and poor material combinations, and can reveal for a given material combination the effect of different preparations of the alloys surface, firing procedure of the ceramic, or the influence of bonding agents on the bond strengths. The numerical analysis is based on the assumptions that both the alloy and the ceramic can be modeled as homogeneous, isotropic, linear-elastic materials and that thermal stresses are not produced in the system during the cooling phase after firing until the temperature drops below the glass transition temperature of the porcelain.

In the numerical study of Lenz et al., viscoelastic effects, which arise from the viscoelastic behavior of ceramic when transforming from rubber state to glass state are ignored. However it is shown in the literature that viscoelastic behavior of ceramics above glass transition temperature greatly influences the transient and residual stress states in metal-ceramic systems. For example, DeHoff et al. [4] used the viscoelastic equations to calculate transient and residual midpoint deflections in bimaterial metal-ceramic strips and compared calculated values with deflection data measured in a beam-bending viscometer. It is concluded that viscoelasticity provides a useful means to estimate the thermal compatibility of metal-ceramic systems. In that study, a viscoelastic finite element model is also constructed and it is seen that viscoelastic finite element method performs reasonably well for predictions of deflection behavior. Another example is due to Haitao Xin *et al.*[5] who mentioned that the viscoelastic behavior of porcelain greatly influenced the thermal residual stress states in metal-ceramic restorations, and that analysis based on elastic behavior could lead to erroneous predictions of stress.

Main objective of this study is to determine the effect of viscoelasticity on thermal residual stresses of metal-ceramic bond three-point flexure specimen. Although there are studies [4, 5, 6, 7] which include the effect of viscoelasticity of ceramic for

metal-ceramic flexure specimen, most of them are concerned only with thermal residual stresses and do not consider viscoelastic effects on the combination of load stresses and residual stresses. In this study three-point flexure bond test was simulated by finite element method. Linear-elastic finite element analyses were performed and results were compared with the studies of Lenz *et. al.* [3, 8] as described in Chapter 2. Then ceramic part was assumed to behave as a viscoelastic material at temperatures greater than the glass transition temperature. Using data from literature [7, 9] a viscoelastic material model was constructed as presented in Chapter 3 . FEA employing viscoelastic material model was carried out and stresses along the metal ceramic interface were predicted. Average stresses were calculated for elastic and viscoelastic FE models in order to determine the effect of viscoelasticity of the ceramic on the bond strength. Viscoelastic finite element model and predictions are described in Chapter 4. Finally, summary, conclusions and future work are presented in Chapter 5.

2. LINEAR ELASTIC ANALYSIS

In this chapter, finite element analysis of a three-point flexure specimen under mechanical and thermal loads is presented. As the main analysis tool, ABAQUS Standard [13] is used. Firstly, a linear-elastic finite element model of the three point bending test including only midpoint load is constructed. Results of this analysis are compared with the results presented in the paper of Lenz *et al.* [3] , which is accepted as the basis of ISO-9693 test [2]. Secondly, thermal residual stresses are analyzed without taking into consideration viscoelasticity of ceramic part. The predictions are compared with theoretical results and results from literature [3, 8, 10].

2.1. Mechanical Load Analysis

Three-point flexure test specimen with dimensions specified in ISO 9693 is shown in Figure 2.1. Both metal and ceramic are modeled as linear elastic with the same material properties as those used in the study of Lenz *et al.* [3].

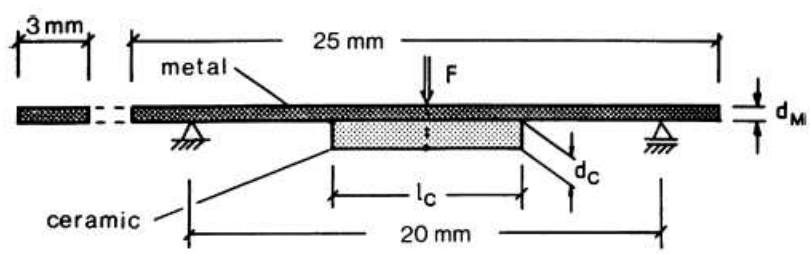

Figure 2.1. Scheme of the three-point flexure bond test. The dimensions of the specimen are given by $l_C = 8mm, d_C = 1mm, d_M = 0.5mm$.
[8]

The Young's modulus (E) and Poisson's (ν) ratios for metal (M) and ceramic (C) parts are

$$E_M = 200 \text{ GPa}, \qquad \nu_M = 0.33$$
$$E_C = 60 \text{ GPa}, \qquad \nu_C = 0.25 \tag{2.1}$$

Because of the symmetry, only one half of the specimen was considered. The mesh consisted of 8-node plane stress quadrilateral elements (CPS8) and is shown in Figure 2.1. Loading consisted of 1N applied at the midpoint of the top surface of the metal. Nodes on the symmetry axis were fixed in the X direction, but were free in the Y direction. At the support, the displacement was fixed in the Y direction, but was free in the X direction.

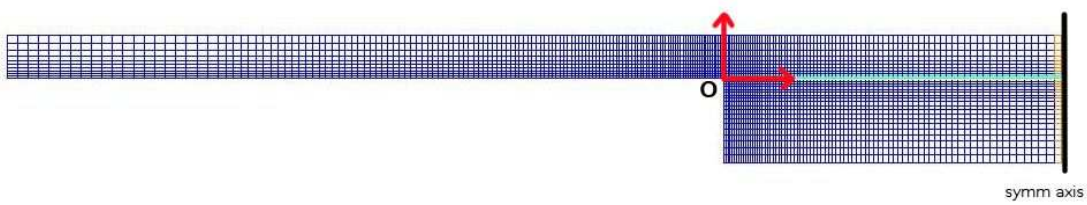

Figure 2.2. Finite element model for linear-elastic analysis

Shear stresses σ_{xy} and normal stresses σ_{yy} resulting from the above model, are shown in Figure 2.3(a). The predictions show the same trend as those of Lenz *et al.* shown in Figure 2.3(b). The quantitative comparison of the results requires determination of the point where the normal stress changes from tension to compression, vicinity of $x = 0.2$mm in Figures 2.3(a) and 2.3(b), and calculation of the average stresses in the vicinity of the metal-ceramic edge. In the following finite element mesh convergence studies for these quantities are presented.

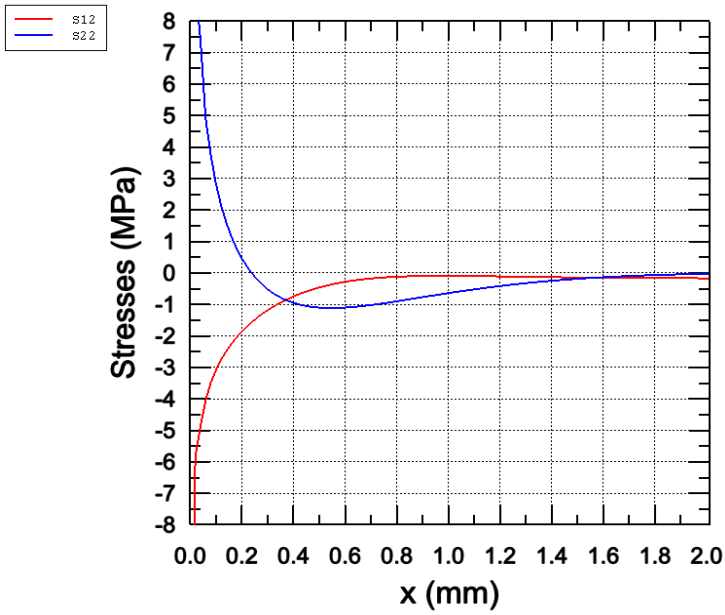

(a) Results of present study.

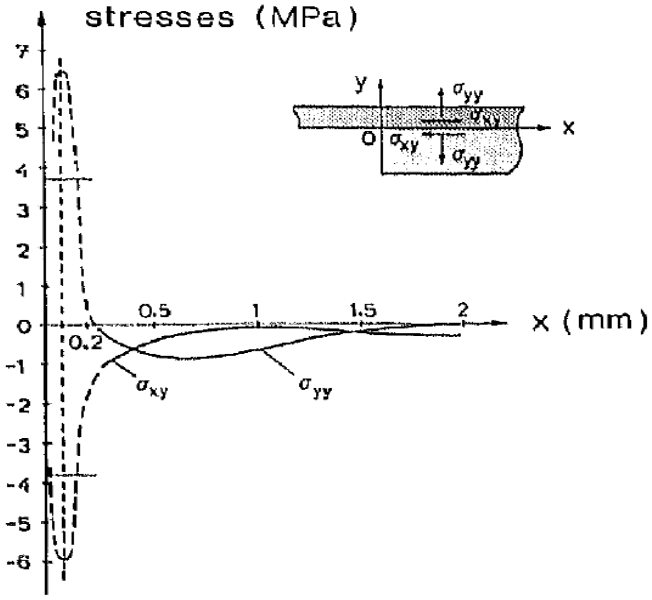

(b) Results of Lenz *et al.* [3]

Figure 2.3. Distribution of shear stress σ_{xy} and normal stress σ_{yy} at the interface. [The dashed line in (b) means that the stresses in the vicinity of the edge ($x = 0.0mm, x \approx 0.2mm$) are not reliable due to the numerical singularity at the edge.]

2.1.1. Convergence Study for x^*

The calculation of average stresses is based on the location where the normal stress changes from tension to compression. The point is denoted by x^* and is located approximately at distance 0.2 mm from the metal-ceramic edge.

The mesh convergence study was performed for both triangular and quadrilateral elements. Since the results are similar for both types of elements, only results for quadrilateral elements are presented in Figure 2.4 and Table 2.1. It can be seen that, for various grid sizes, the point where normal component of the stress changed direction (x^*) approaches 0.23. Although results for CPS4, 4-node bilinear plane stress elements give satisfactory results, since there is not much difference in computational time , using CPS8, 8-node biquadratic plane stress elements, is preferred since these elements are known to have superior convergence and to yield more accurate solution.

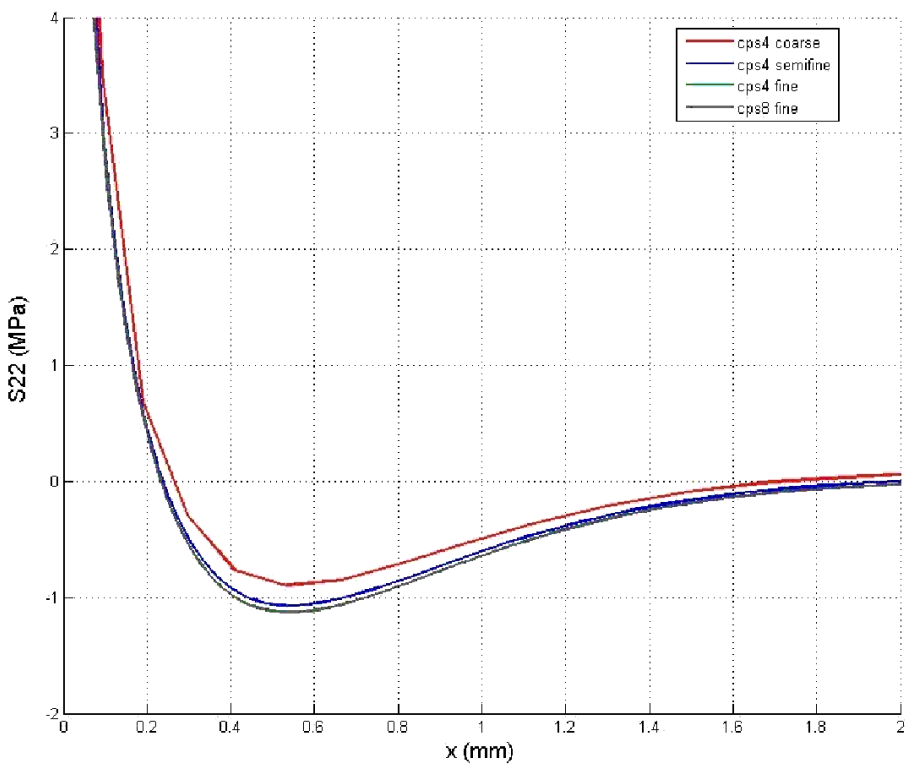

Figure 2.4. Mesh convergence study for x^*.

Table 2.1. Mesh convergence study for value of x^* for quadrilateral elements. CPS4:4-node bilinear plane stress, CPS8:8-node biquadratic plane stress

Plane Stress	CPS4			CPS8
	Coarse	Semifine	Fine	Fine
# of Elements	352	3800	60800	60800
# of Nodes	452	4132	62122	185042
x*	0.2642	0.2387	0.2333	0.2335

2.1.2. Convergence Study for Edge Stresses

Due to a singularity, stresses near the edge are not reliable. Although these stresses are not used directly, they are part of the calculation of the average stresses near that edge, therefore an accurate determination of these stresses is important. Therefore mesh convergence study was performed for the stresses in the vicinity of the edge ($x = 0.0, y = 0.0$). The mesh shown in Figure 2.1 was refined in the vicinity of the edge as shown in Figure 2.5. 40, 80, 160 and 320 biased elements were used in that region (0-0.4mm) and results are presented in Figures 2.6 and 2.7.

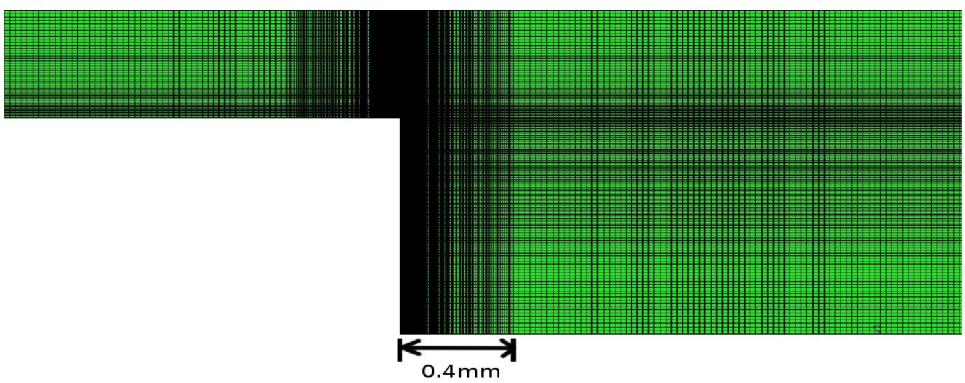

Figure 2.5. Mesh convergence study in the vicinity of the point $x = 0.0, y = 0$.

As seen from Figure 2.6 stresses in the vicinity of the edge overlap until $x =$ 0.01mm for all models. Even the model having a uniform element length of 0.025mm gives reasonable results in the unreliable region $x = 0.0, x = 0.2$ (Figure 2.7).

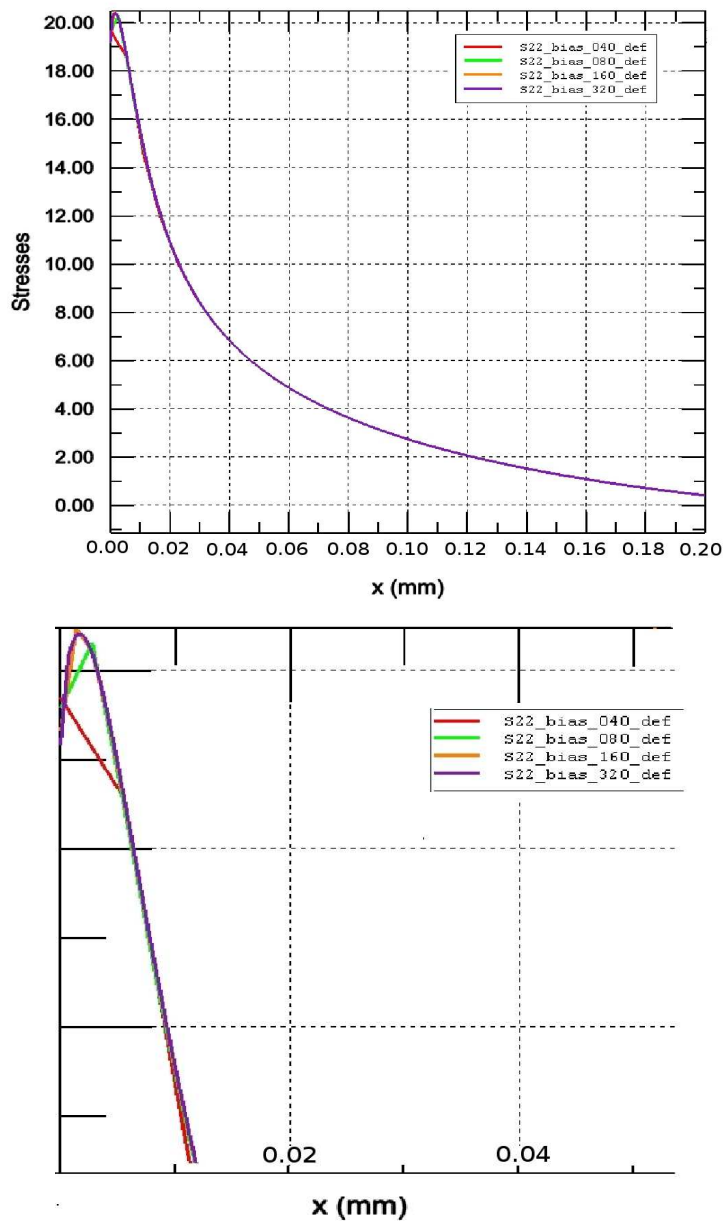

Figure 2.6. Mesh convergence study in the vicinity of the edge.

S12 : σ_{xy}, S22 : σ_{yy}

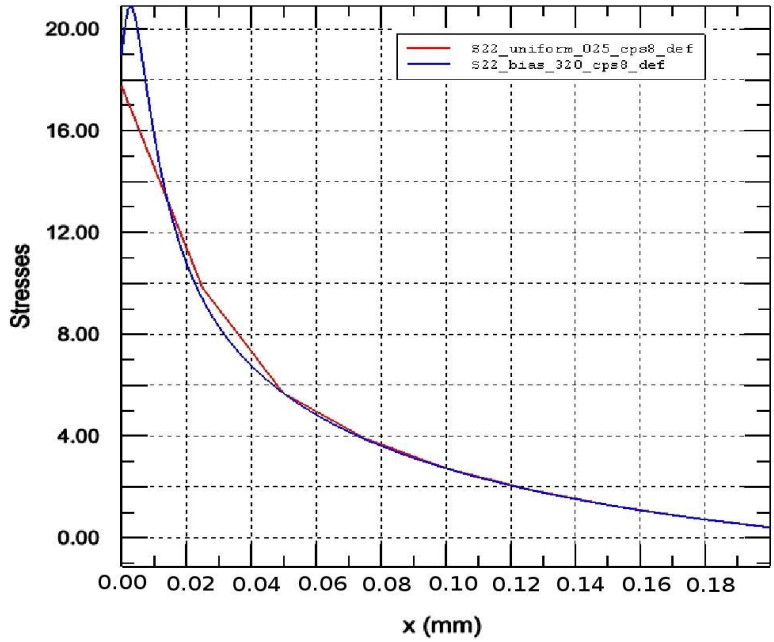

Figure 2.7. Mesh convergence study in the vicinity of the point $x = 0.0, y = 0.0$ (uniform mesh (el. size:0.025mm) vs biased mesh)

2.1.3. Average Stresses

Even though the stress distribution near the edge of metal-ceramic interface is of importance, due to the numerical singularity of this point computed values are less reliable. The method presented in the paper of Lenz *et al.* [3] allows the calculation of mean values independent of the precise stress distribution at the edge. In this method, average values of stresses are determined for the region between $x = 0$, the edge, and x^*, the point where σ_{yy} changes direction. In particular the calculated interface stresses along $y = 0$ beyond the point of zero normal stress (x^*) and those along the intersection $x = 4$ are used to compute the mean values $\overline{\sigma}_{xy}$ and $\overline{\sigma}_{yy}$ such that equilibrium is established for the semi-layer. Since this method involves only stresses at points farther from the critical point $x = 0$, it is more reliable. In analytical form, the equilibrium of forces that defines these mean values (using symmetry of stress tensor, i.e., $\sigma_{xy} = \sigma_{yx}$) is given by equations (2.2) and (2.3).

$$\frac{1}{b}\sum F_x = \underbrace{\int_{x=0}^{x^*} \sigma_{xy}\left(x, y=0\right) dx}_{\overline{\sigma}_{xy}} + \int_{x=x^*}^{l_c/2} \sigma_{xy}\left(x, y=0\right) dx + \int_{y=0}^{-d_c} \sigma_{xx}\left(x=\frac{l_c}{2}, y\right) dy = 0 \tag{2.2}$$

$$\frac{1}{b}\sum F_y = \underbrace{\int_{x=0}^{x^*} \sigma_{yy}\left(x, y=0\right) dx}_{\overline{\sigma}_{yy}} + \int_{x=x^*}^{l_c/2} \sigma_{yy}\left(x, y=0\right) dx + \int_{y=0}^{-d_c} \sigma_{xy}\left(x=\frac{l_c}{2}, y\right) dy = 0 \tag{2.3}$$

In numerical evaluation of these equations 2.2 and 2.3 the values of σ_{xy} and σ_{yy} came from finite element stress output. Alternative way of calculating average stresses is through the use of nodal forces. Equations (2.2) and (2.3) are then replaced by equations (2.4) and (2.5).

$$\sum_{x=0}^{x=x^*} F_x + \sum_{x=x^*}^{x=l_c/2} F_x + \sum_{y=-d_c}^{y=0} F_x = 0 \tag{2.4}$$

$$\sum_{x=0}^{x=x^*} F_y + \sum_{x=x^*}^{x=l_c/2} F_y + \sum_{y=-d_c}^{y=0} F_y = 0 \tag{2.5}$$

In the above equations the values of F_x and F_y are the finite element internal nodal force output.

In Figure 2.8 stresses calculated from nodal force output and stress output at the metal-ceramic interface are compared. It can be seen from the figure that solutions are the same. In the rest of the analysis nodal force outputs are used in determination of average stresses and bond strengths.

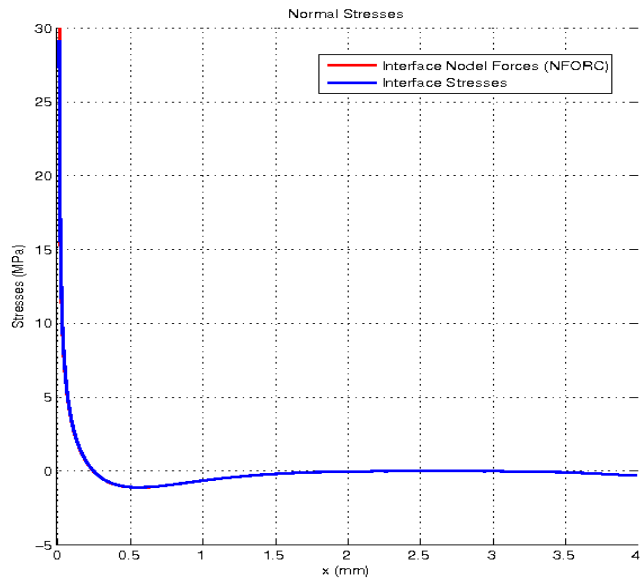

(a) Normal Stresses

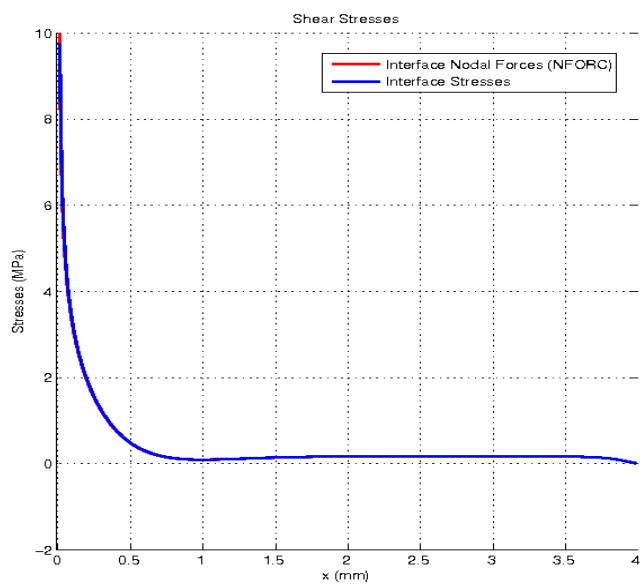

(b) Shear Stresses

Figure 2.8. Comparison of stresses : Finite element stress output and stresses calculated using internal nodal forces.

2.1.4. Comparison of Two Models

The main objective of linear elastic analysis is the verification of the finite element model against the results presented by Lenz. The comparison was focused on the average stresses and the ratio of the average stresses for a range of metal Young's moduli.

Lenz reports:

- for $E_M = 200\text{GPa} \quad E_C = 60\text{GPa} \quad \nu_M = 0.33 \quad \nu_C = 0.25$

  $\overline{\sigma}_{xy} = 3.78$

  $\overline{\sigma}_{yy} = 3.75$

  $\left|\frac{\overline{\sigma}_{xy}}{\overline{\sigma}_{yy}}\right| = 1.008$

  $x^* \approx 0.2$
- for 80 GPa $\leq E_M \leq$ 220 GPa

  $\left|\frac{\overline{\sigma}_{xy}}{\overline{\sigma}_{yy}}\right| \approx 1$

  which is reqiured to ensure that all metal-ceramic combinations are tested under similar loading conditions.

The results of the FE model of the present study are as following:

- for $E_M = 200\text{GPa} \quad E_C = 60\text{GPa} \quad \nu_M = 0.33 \quad \nu_C = 0.25$

  $\overline{\sigma}_{xy} = 3.57$

  $\overline{\sigma}_{yy} = 4.39$

  $\frac{\overline{\sigma}_{xy}}{\overline{\sigma}_{yy}} = 0.81$

  $x^* \approx 0.23$
- for 80 GPa $\leq E_M \leq$ 220 GPa, x^* and $\left|\frac{\overline{\sigma}_{xy}}{\overline{\sigma}_{yy}}\right|$ values are plotted against E_M in Figure 2.9(a) and it is seen that x^* varies between 0.2 and 0.25, and calculations show that varying x^* in this range, $\overline{\sigma}_{xy}$, $\overline{\sigma}_{yy}$, hence their ratio change. As seen in Figure 2.9(b) $\left|\frac{\overline{\sigma}_{xy}}{\overline{\sigma}_{yy}}\right|$ takes values between 0.9 and 0.8. Predictions of the present model differ from that of Lenz in location of x^*, as well as the dependence of $\left|\frac{\overline{\sigma}_{xy}}{\overline{\sigma}_{yy}}\right|$ on E_M.

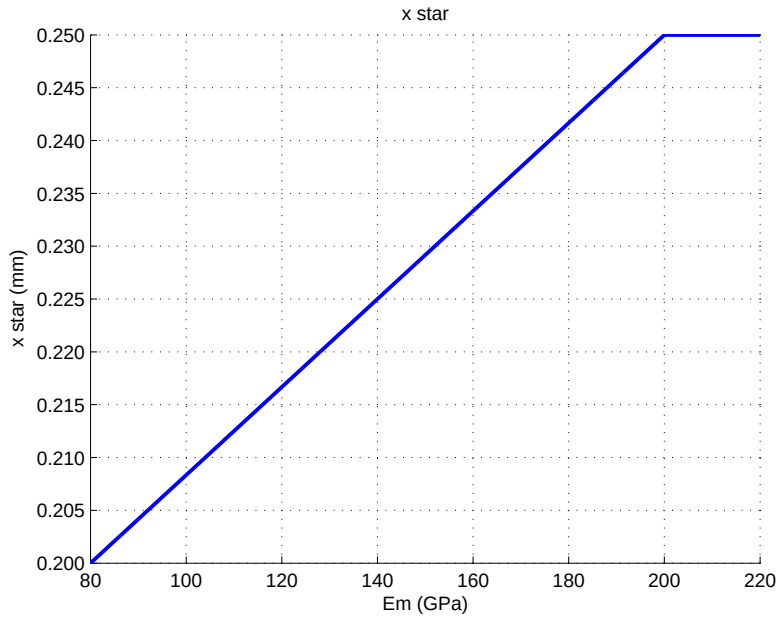

(a) x^* vs Em

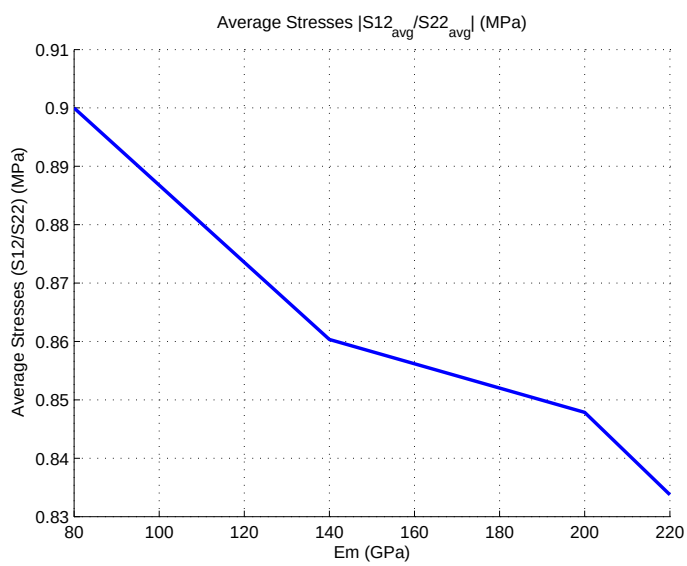

(b) $\left|\frac{\overline{\sigma}_{12}}{\overline{\sigma}_{22}}\right|$ vs Em

Figure 2.9. x^* and $|\sigma_{xy}/\sigma_{yy}|$ with respect to Em

As stated before the present FEM was expected to give the same results for average stresses as that of Lenz's model. The discrepancy could be explained by the sensitivity of the finite element mesh to the stress values. Numerical integration used in finite element calculations and stress postprocessing may also contribute to this discrepancy.

The values reported for the present study were confirmed through a convergence study and by calculating average stresses using two different methods. At this point it should be noted that there is at least one other study (Griggs *et al.*) [12] where it is claimed that $\left|\frac{\overline{\sigma}_{xy}}{\overline{\sigma}_{yy}}\right|$ is not close to 1.

2.2. Thermal Load Analysis

Due to the fabrication process, all PFM restorations are loaded with thermal stresses, which develop during cooling phase after firing because of the difference in the coefficients of thermal expansion of the two materials. It is therefore desirable to be acquainted with the distribution of residual thermal stresses along the bond interface. In this section a finite element analysis of a three-point flexure specimen for thermal loading is performed. This type of analysis allows determination of residual stresses which is essential for viscoelastic analysis.

It should be noted that for the three-point flexure test the coordinate system used in this section is not the same as the one used in the mechanical load analysis section (2.1). For a direct comparison of the results with studies from the literature the coordinate system presented in Figure 2.10(b) will be used in the rest of this study.

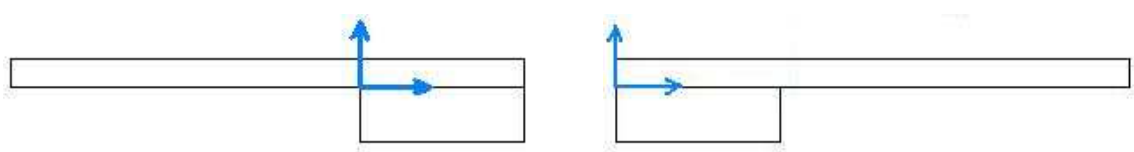

(a) Three-point flexure test geometry used in Section 2.1 and in the study of Lenz *et al.* [3]

(b) Three-point flexure test geometry used in the rest of this study.

Figure 2.10. Different coordinate systems used in three-point flexure test models.

Both ceramic and metal are assumed to be linear-elastic (viscoelastic effects are ignored). It is also assumed that thermal stresses are not produced in the system during the cooling phase after firing until the temperature drops below the glass transition temperature of the porcelain. Material properties for the ceramic are [8]

$$E_C = 60GPa, \qquad \nu_C = 0.25$$

For the metal part various Young's moduli and a constant Poisson's ratio are used as

$$E_M = 80GPa, 140GPa, 220GPa, \qquad \nu_C = 0.25$$

The magnitude of the thermal stresses depends on $\Delta\alpha = \alpha_M - \alpha_C$ the difference between the coefficient of thermal expansion of the metal, α_M, and that of ceramic, α_C on the interval ($\Delta\Theta = \Theta_R - \Theta_G$) between ambient temperature, Θ_R, and the glass transition temperature, Θ_G of the porcelain. The following values are used in the present study.

$$\Delta\alpha = \alpha_M - \alpha_C = 1\text{x}10^{-6}K^{-1}$$
$$\Delta\Theta = \Theta_R - \Theta_G = -550^o\,C \tag{2.6}$$

corresponding to

$$\Theta_R = 25^oC, \text{ and } \Theta_G = 575^oC$$

The predictions are compared with those of Lenz *et al.* [8] in Figures 2.13 and 2.14. In Figure 2.13 the distribution of bending stress , σ_{xx}, at various locations along the interface ($x = 4$ mm marks the end of the ceramic layer) are presented. According to St. Venant's principle, it is expected that the bending stresses calculated with the aid of Timoshenko's theory of bimaterial strips [10], where the metal substrate is completely covered with porcelain, should practically coincide in the middle of the structure ($x = 0$) with those calculated numerically for the specimen. In Figures 2.13(a,b) Lenz's and Timoshenko's results, and results of the present thermal analysis are shown. In Figure 2.14 distribution of thermal shear and normal stresses along the bond interface are presented. The results are in very good agreement with the results of Lenz *et al.* [8].

In the paper of Lenz *et al.*, authors combined the results of thermal analysis with the results of their previous study [3] for mechanical load, and they concluded that with regard to the average stresses $\overline{\sigma}_{xy}$ and $\overline{\sigma}_{yy}$, the immediate vicinity of the point of debonding is subject to a thermal shear/compression system, whereas the load applied in the bond test leads to a shear/tension stress state (Figure 2.11). Based on Figure 2.11 Lenz says that for combined loading there is an increase in shear stress, while the tensile stress is offset by a compressive thermal stress. However it seems that the difference in coordinate systems used in calculating thermal and load stresses is not accounted for in Figure 2.11. When the correct transformation is used, shear stresses due to mechanical load and thermal load become of opposite sign, hence overall shear stress is reduced (Figure 2.12). As a consequence, normal stresses may play important role in determination of the bond strength. This in turn may require modification of the definition of bond strength in terms of the average shear stress as assumed by Lenz.

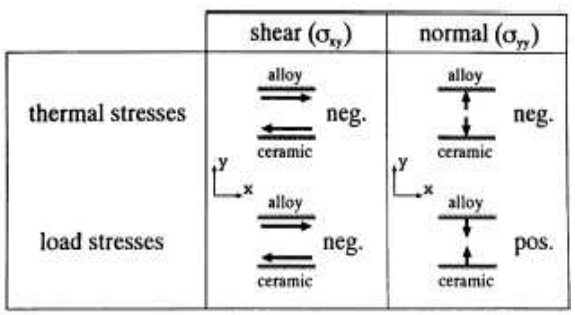

Figure 2.11. Results of Lenz *et al.* [8]

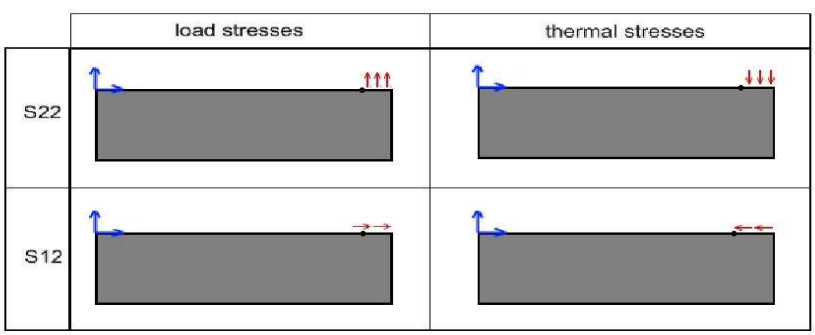

Figure 2.12. Results of present study

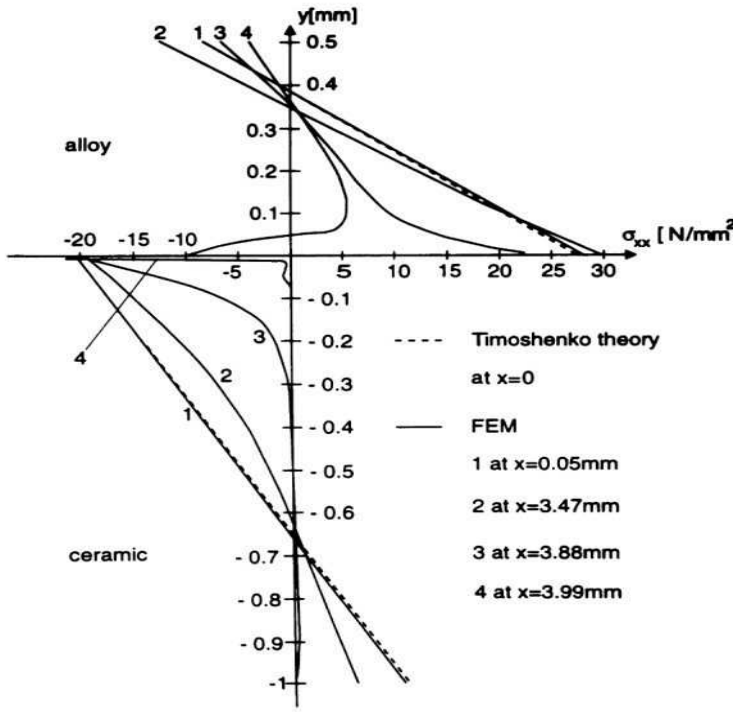

(a) Results of Lenz *et. al.*. [8]

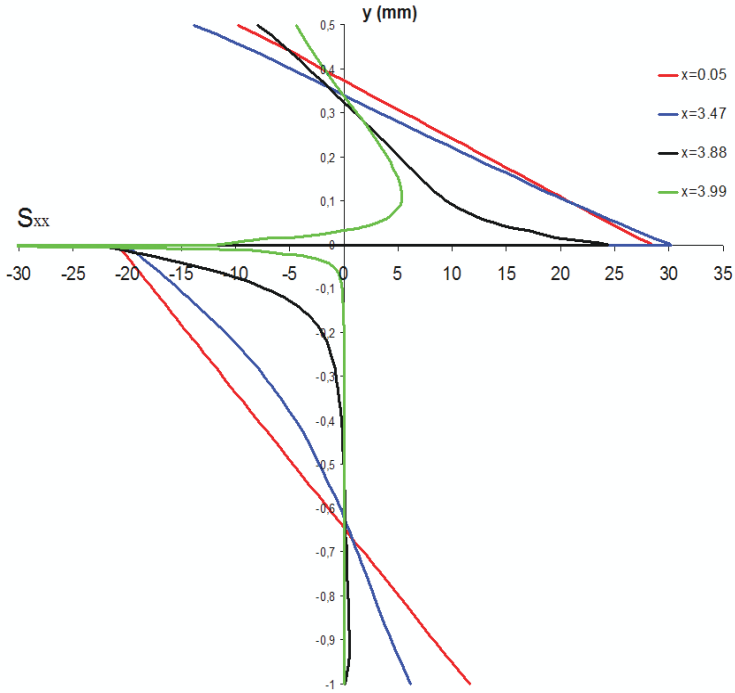

(b) Results of present study

Figure 2.13. Distributions of thermal stresses at four sections of specimen.

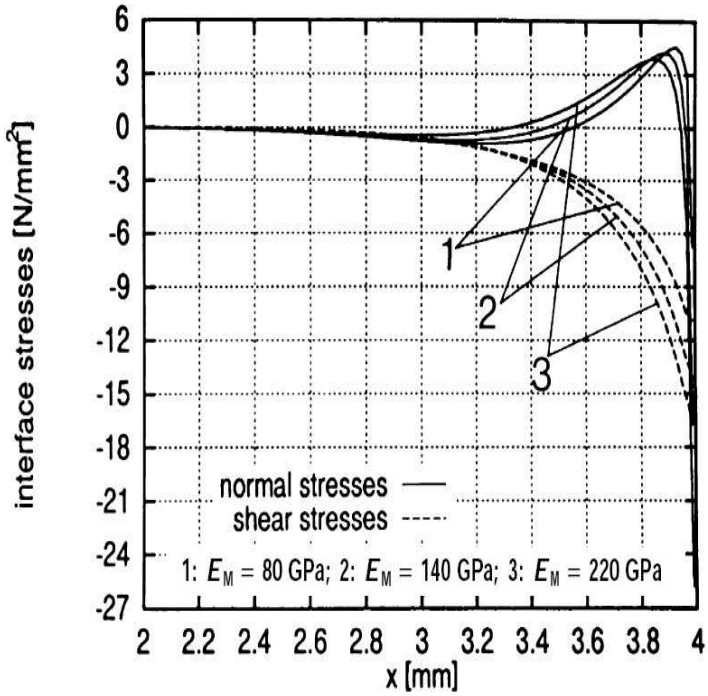

(a) Results of Lenz *et. al.*. [8]

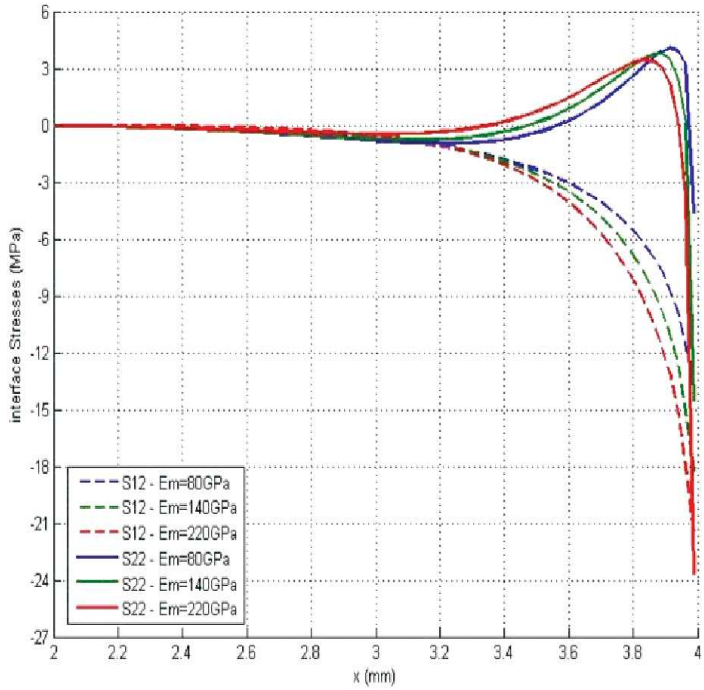

(b) Results of present study

Figure 2.14. Distribution of thermal shear and normal stress along the bond interface

3. VISCOELASTIC MATERIAL MODEL

A number of investigators have recognized that the residual stress state in metal-ceramic dental restorations depends on many factors, including contraction mismatch, cooling rate, firing temperature, geometry and fabrication techniques. To account for the effect of cooling rate or temperature distribution on stress development, it is necessary to model the ceramic as a viscoelastic material, which in turn requires the determination of the time-dependent material properties of ceramic at high temperature. To represent these properties data presented in papers [7, 9] are used and the master relaxation curve and the shift function are constructed.

3.1. Relaxation Moduli at a Uniform Temperature

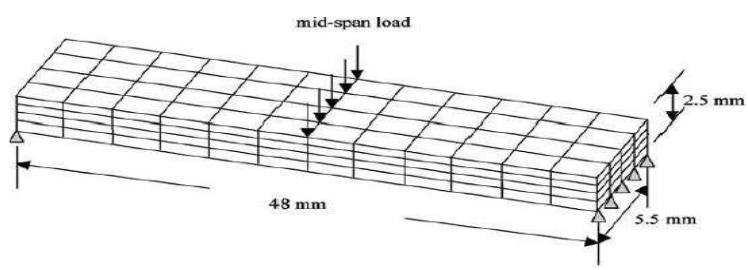

Figure 3.1. Finite element model of the three-point bending specimen used in the analysis of DeHoff *et. al.*. [7]

DeHoff and Anusavice ([6]) used a beam-bending-viscometer (BBV) to measure creep behavior from which creep functions were calculated for different porcelains at the temperatures ranging from 450°C to 650°C. In another study, DeHoff and Anusavice [7] used these creep functions for determination of the shear relaxation functions through the use of Laplace transform methods and linear viscoelastic theory since shear relaxation functions are more suitable for many FEA application (see Figure 3.1).

For validation of the relaxation moduli, FE model of a BBV used in [6, 7] was constructed in ABAQUS and results were compared with the results of DeHoff *et*

al [6, 7]. The applied midpoint load, P, was calculated from

$$P = \frac{12bh^3\eta_s C}{L^3} \tag{3.1}$$

where;

P : applied midpoint load,

η_s: shear viscosity,

C: creep rate,

L, b, h : Length, width and height of the specimen

Using dimensions given in Figure 3.1, and $\eta_s = 1.715 \cdot 10^5, \quad C = 1.232 \cdot 10^{-3}$ given in [7] $P = 1.9702$N was obtained.

The shear relaxation modulus was represented by a four-term Prony series as

$$G(t) = G_1 e^{-\frac{t}{\tau_1}} + G_2 e^{-\frac{t}{\tau_2}} + G_3 e^{-\frac{t}{\tau_3}} + G_4 e^{-\frac{t}{\tau_4}} \tag{3.2}$$

It's known that dilatational relaxation has a minor effect on stress calculations for most stress states . Therefore, the dilatational behavior of dental ceramics has been assumed to be elastic and bulk modulus was taken constant as

$$K(t) = K_0 \tag{3.3}$$

Since there is no material and geometry dependence in the z-direction (see Figure 3.1), instead of using 3D elements, 2D quadrilateral plane stress elements were used. The mesh is shown in Figure 3.2. Shear relaxation constants for 550^oC are tabulated

in Table 3.1.

Midpoint deflection for $P = 1.9702N$ is shown in Figure 3.3.and compares very well with the results in [7].

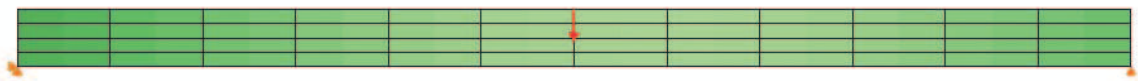

Figure 3.2. Properties of FE Model: CPS8 Elements, $P_1 = 1.9702N$

Table 3.1. Material constants.

Temp (^oC)	G_1	G_2	G_3	G_4	τ_1	τ_2	τ_3	τ_4
550	20640	2684	720	102	2.7	17.1	67	323

$K(0)$	36598
$G(0)$	24146
$E(0)$	59379

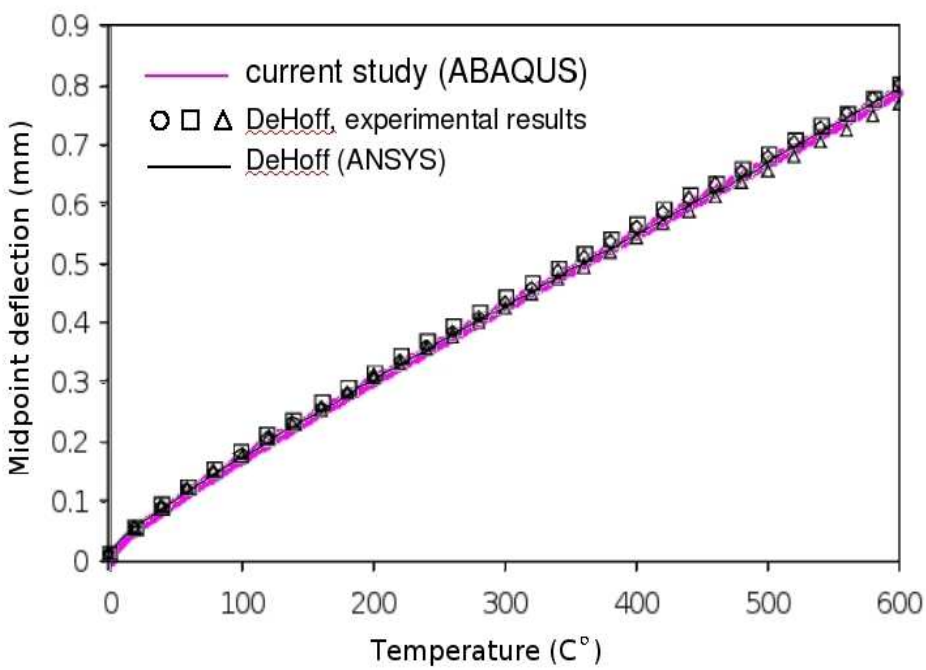

Figure 3.3. Midpoint deflection versus time at 550^oC for $P = 1.9702N$.

3.2. Master Relaxation Modulus

Since it is known that dental ceramics used in this study exhibit thermologically simple behavior over the temperature range interested, it is possible to determine the shift function and the master curve using the data presented in [7, 9]. Reference temperature was taken as 550^oC and relaxation curves at different temperatures (525^oC, 575^oC, 600^oC) were shifted to form a single curve.

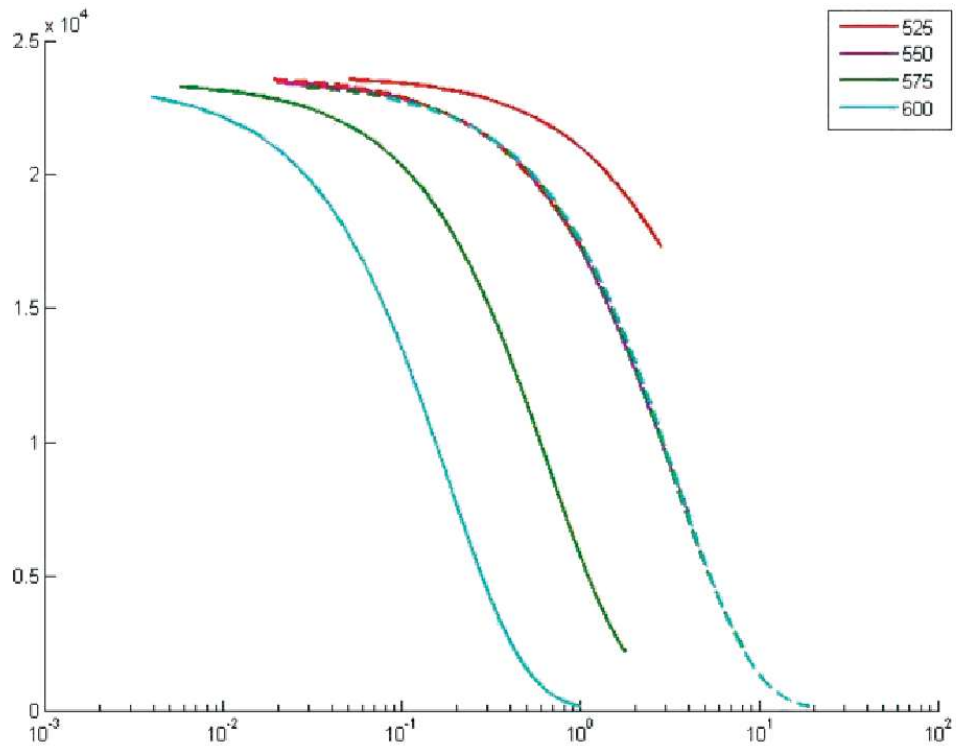

Figure 3.4. Determination of shift values a_T

Resulting a_T values were

$$a_T(525) = 10^{0.45}$$
$$a_T(575) = 10^{-0.68}$$
$$a_T(600) = 10^{-1.28} \tag{3.4}$$

Using the shift values given in (3.4) a master relaxation curve, $G(t)$, was constructed using Matlab curve fitting toolbox. Resulting function is seen in Figure 3.5.

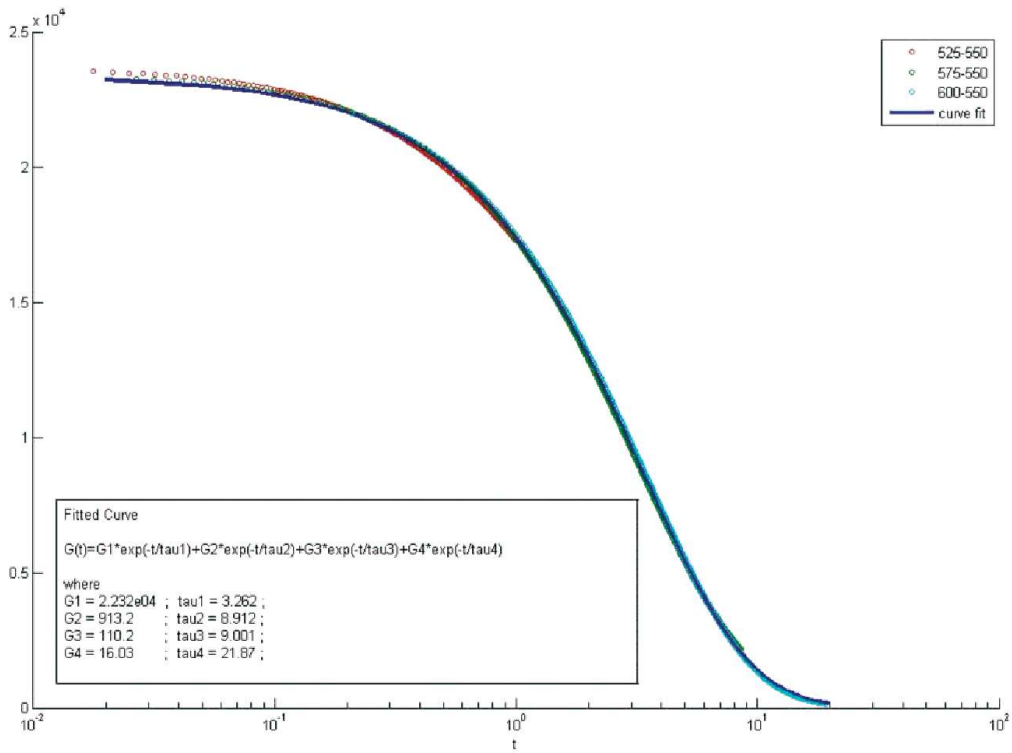

Figure 3.5. Master relaxation curve at reference temperature 550^oC

Table 3.2. Constants of master relaxation curve at reference temperature 550^oC.

Temp (^oC)	G_1	G_2	G_3	G_4	τ_1	τ_2	τ_3	τ_4
550	22320	913.2	110.2	16.03	3.262	8.912	9.001	21.87

Williams-Landell-Ferry [14] form was fitted to the shift function shown in Figure 3.5 using optimization toolbox of Matlab. Results are given in equation 3.5 and shown in Figure 3.6.

$$\log(a_T) = -\frac{C_1(T - T_{ref})}{C_2 + (T - T_{ref})} \tag{3.5}$$

where

$$C_1 = -4.5474$$

$$C_2 = -227.6316 \tag{3.6}$$

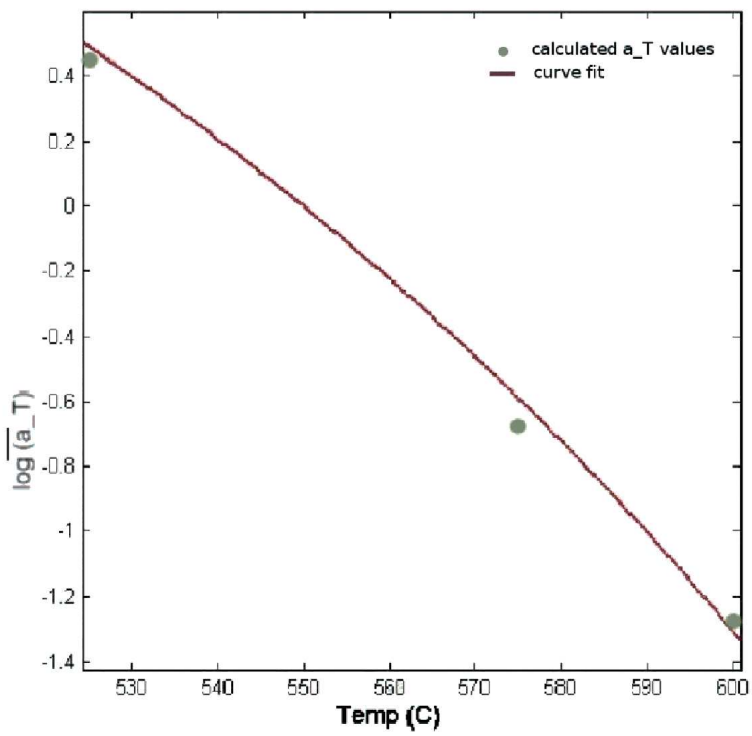

Figure 3.6. Curve fit for shift values at $T_{ref} = 550^o$C.

Master relaxation function, $G(t)$, and WLF constants C_1, C_2 were used in the construction of viscoelastic finite element model described in the next chapter.

4. VISCOELASTIC FINITE ELEMENT ANALYSIS

In the previous section both linear and viscoelastic finite element models for three point bending test of a metal-ceramic specimen were constructed and verified against results from literature [3, 8, 7]. Additionally the relaxation data at various temperatures reported in literature were used to construct a master relaxation curve and a shift function in order to represent viscoelastic material model at all temperatures.

In this section, the effect of viscoelasticity on residual stresses at the metal-ceramic interface are examined. Since dental metal-ceramic restorations are also exposed to mechanical loads, combined stresses should be considered. Therefore stresses under unit midpoint load $P = 1N$ and $P = 10N$ load are calculated. 10N was selected since this load ensures that the metal-ceramic combination has a bond strength greater than 25 MPa, which is the minimum value specified in ISO 9693 [2].

The finite element model was implemented in two steps. In the first step a thermal analysis was performed. This analysis simulates free convective cooling of the specimen in the BBV furnace from 700^oC to 25^oC. It was assumed that thermal gradients do not exist in the metal-ceramic system. Nodal temperatures were calculated at a set number of time steps and these temperatures served as the input thermal loading for the structural analysis which was in the second step. The structural model consisted of three solution steps: cooling process from 700^oC to 550^oC with viscoelastic elements for the ceramic part, cooling process from 550^oC to 25^oC with elastic elements for both ceramic and metal parts, and application of midpoint load.

Details of the finite element model for thermal and structural analysis are as following:

Step I : *Thermal Analysis*

$\alpha_M = 1.51 \cdot 10^{-5}$ (Thermal expansion coefficient of metal)

$\alpha_C = 1.41 \cdot 10^{-5}$ (Thermal expansion coefficient of ceramic)

$\Theta_R = 25^o$C (ambient temperature)

$\Theta_i = 720^o$C (initial temperature)

Element type : DC2D8 (8-node biquadratic diffusive heat transfer element)

Number of elements : 16400

Number of nodes : 50321

Step II : *Structural Analysis*

E_M : 140000 MPa $\quad \nu_M$: 0.33

E_C : 59379 MPa $\quad \nu_C$: 0.229

G_1 : 0.9555, $\quad G_2$: 0.039093, $\quad G_3$: 0.0047176, $\quad G_4$: 0.00068623

τ_1 : 3.262, $\quad \tau_2$: 8.912, $\quad \tau_3$: 9.001, $\quad \tau_4$: 21.87

Element type : CPS8 (8-node biquadratic plane stress element)

Number of elements : 16400

Number of nodes : 50321

4.1. Thermal Residual Stresses

In Figure 4.1 residual stresses for elastic and viscoelastic models are presented. As can be seen in the figure viscoelastic residual stresses are smaller than elastic stresses, which means that elastic model is more conservative and can lead to overestimated prediction of residual stresses.

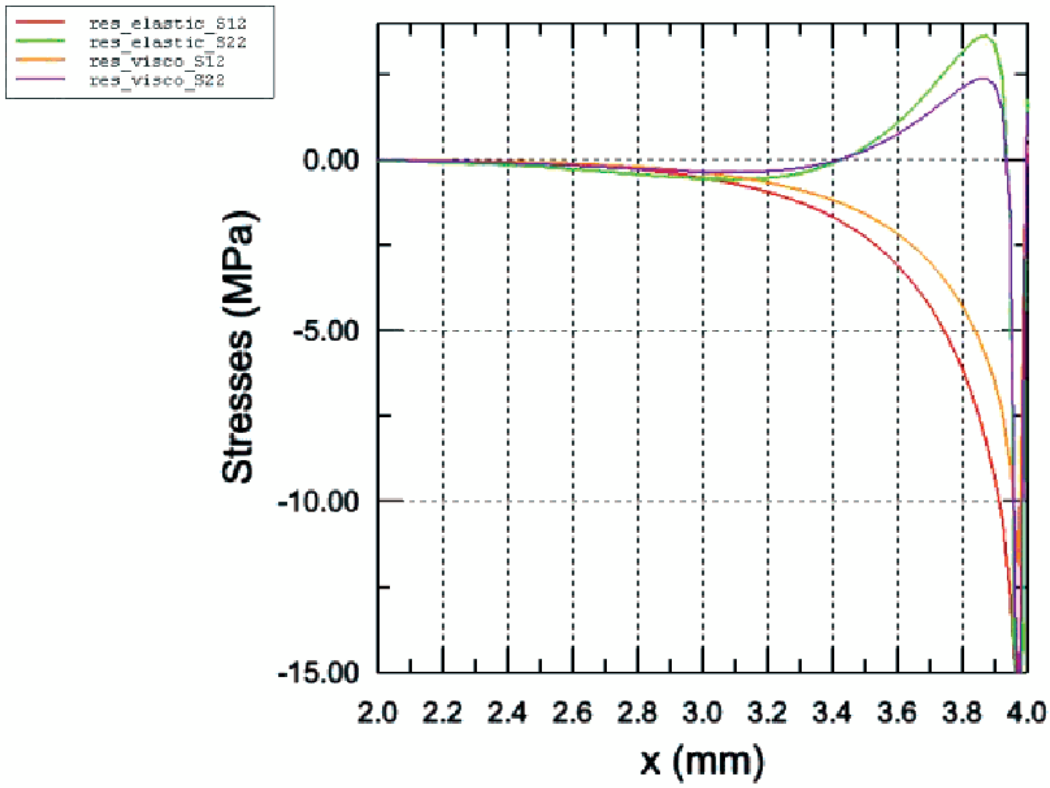

Figure 4.1. Viscoelastic and Elastic Residual Stresses

4.2. Thermal Residual and Mechanical Load Stresses

In Figure 4.2 load stresses for $P = 1$N case and thermal residual stresses along the interface are compared. In Figure 4.3 superposition of load stresses and residual stresses for elastic and viscoelastic models are presented. As seen from Figure 4.2, directions of load stresses and residual stresses are opposite (load stresses positive, residual stresses negative). In order to determine whether shear and/or normal stresses are critical for debonding, average stresses in the vicinity of the edge $x = 4.0, y = 0$ for combined mechanical and thermal loads (Figure 4.3) should be taken into account.

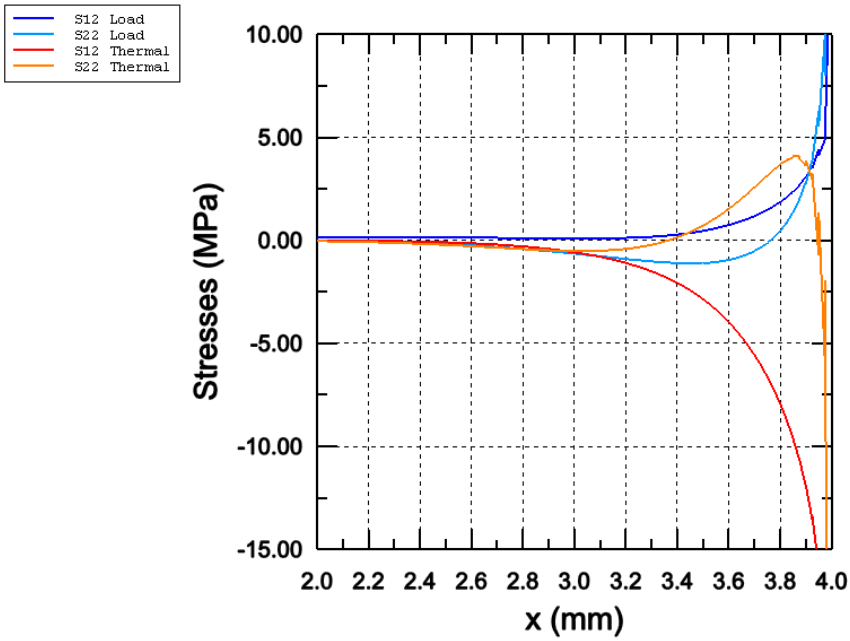

Figure 4.2. Thermal Residual (Viscoelastic) and Mechanical Load Stresses (1N)

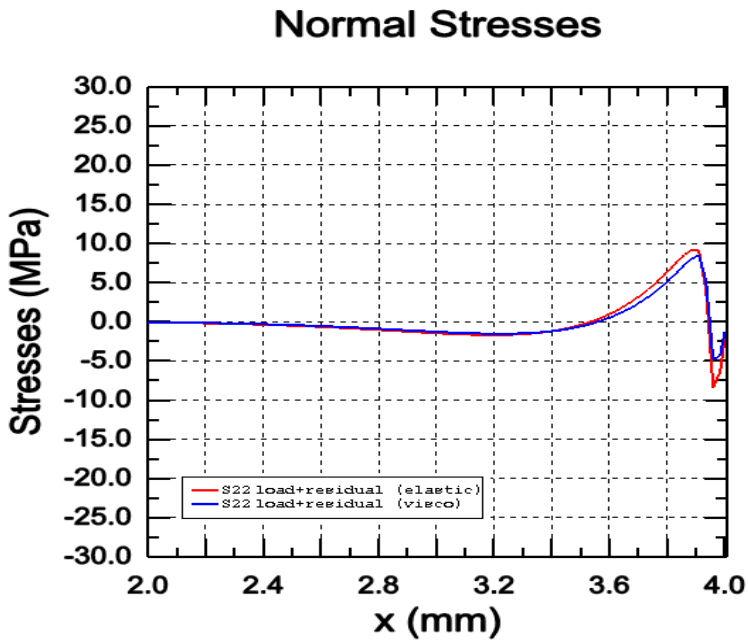

(a) Normal Stresses

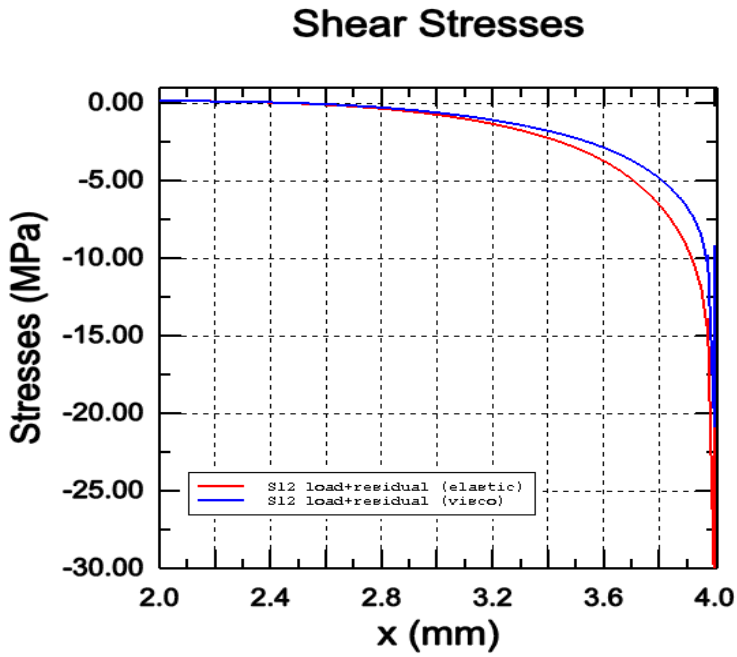

(b) Shear Stresses

Figure 4.3. Superposition of Mechanical Load Stresses (1N) and Residual Stresses (Viscoelastic and Elastic)

4.3. Bond Strength

ISO 9693 defines the bond strength as

$$\tau_b = |\overline{\sigma}_{xy}| F_{fail} \qquad \text{(MPa)} \tag{4.1}$$

where $|\overline{\sigma}_{xy}|$ is the average shear stress and F_{fail} is the load under which debonding starts at the ceramic-metal edge of a three-point flexure specimen. This definition is due to Lenz [3] who calculated $|\overline{\sigma}_{xy}|$ from a linear elastic finite element analysis of the flexure specimen under unit load. The notation for the bond strength definition (4.1) $|\overline{\sigma}_{xy}|/|\overline{\sigma}_{yy}| \approx 1$ as calculated from the finite element analysis.

In the present study, the effect of thermal load and viscoelastic behavior on the stres, hence the bond strength, was investigated.

Table 4.1. Average stress for elastic and viscoelastic analyzes.

Average Stress $\overline{\sigma}$		$\overline{\sigma}_{xy}$	$\overline{\sigma}_{yy}$
Residual	Viscoelastic	-11.26	0.51
	Elastic	-14.14	0.83
Load (Visco=Elastic)	$F = 1N$	4.07	4.72
	$P = 10N$	40.71	47.20
Residual+Load ($P = 1N$)	Viscoelastic	-7.19	5.25
	Elastic	-10.07	5.56
Residual+Load ($P = 10N$)	Viscoelastic	29.45	47.83
	Elastic	26.57	48.15

The average stresses calculated in this study are given in Table 4.1. Residual stresses, load stresses and combined stresses are presented for both elastic and viscoelastic analyzes. According to Table 4.1:

- Residual shear stresses are much higher than residual normal stresses. This is in agreement with literature.

- Predictions for superimposed residual and load stresses do not scale proportional to the applied load as it is the case when only load stresses are considered. For a small load, P=1N, combined shear stresses are higher than combined normal stresses. When high loads are considered, P=10N, normal stresses become higher than shear stresses.
- Viscoelasticity has a considerable effect on the calculated average stresses.

Based on the above observations, it would be more realistic to calculate bond strength taking into account both normal and shear stresses. Modification of the bond strength definition given in (4.1) requires further analysis and may be subject of a future work. One possible approach is be to use a combination of experiment and computational model. In such an approach for a given metal-ceramic system failure load is measured in three point flexure. Then a viscoelastic finite element analysis that takes into account residual stresses is performed for the measured failure load and average stresses are calculated. These value are then used to determine the bond strength. Although the cost of such a method would be slightly higher than the current ISO 9693 the results would be more accurate.

5. CONCLUSIONS

The objective of this thesis was to study the effects of viscoelasticity on stress distribution and bond strength of dental metal-ceramic restorations. In order to determine these effects, elastic and viscoelastic finite element models were constructed and results for mechanical load stresses, residual stresses and superposition of load and residual stresses were compared with each other.

In the first part of the thesis, three point bending test was simulated using finite element method. Main aim of this section was to validate the elastic (both ceramic and metal parts were assumed to be elastic materials) finite element model for mechanical and thermal loadings. Firstly only a unit midpoint load was applied and stresses along the metal-ceramic interface were investigated. Outcome of this analysis was the location of the point where normal stress changes direction and based on this location, average stresses and bond strengths over the critical region were calculated. Secondly, thermal residual stresses which originate because of the difference in thermal contraction coefficients were investigated.

In the second part of this thesis, relaxation data at various temperatures reported in literature were used to construct a master relaxation curve and a shift function in order to represent viscoelastic material model for the ceramic at all temperatures. Using this model finite element analysis was performed and residual stress at the metal-ceramic interface were examined. Since dental metal-ceramic restorations are exposed to mechanical loads, stresses under various loads coupled with thermal loading were calculated for both elastic and viscoelastic models. The results indicate that for the combined thermal and mechanical loading average normal stress is higher than average shear stress. Therefore defining bond strength in terms of shear stress only may be incorrect and consideration of the normal stress as well may be necessary. The study also shows that viscoelasticity has a considerable effect on the calculated average stresses, hence it should be taken into account in the determination of the bond strength.

Several simplifying assumptions were made in this study, and caution should be taken in interpretation of the results. The fundamental assumption that porcelain can be characterized as a linear visco-elastic material has not yet been supported with experimental evidence. It seems likely that the linear assumption is valid at the higher temperatures, but it may not be valid throughout the entire temperature range over which time-dependent behavior occurs. Since there is not enough data about temperature profiles for porcelain-metal systems during cooling, it is assumed that thermal gradients do not exist in the porcelain-metal system. This restricts the application of the model presented in this study to systems that are cooled rather slowly or to systems for which only small thermal gradients develop during normal cooling. Finally, the model developed in this study is based on a bimaterial strip consisting of a visco-elastic layer (body porcelain) and an elastic layer (metal). However it should be known that the clinical situation involves layers of incisal porcelain, body porcelain, opaque porcelain, and a metal substrate.

In spite of these limitations, it is clear that the thermal residual stresses are very important to metal-ceramic restorations, and they are greatly affected by the viscoelastic behavior of porcelain.

Future studies can be concentrated on a realistic dental metal-ceramic restoration. A 3D model of dental restoration, which includes opaque porcelain layer and bonding agent layer can be analyzed and more accurate results for residual and load stresses can be obtained. A fracture analysis can be also useful in determination of the bond strength.

REFERENCES

1. DeHoff P H, K J Anusavice and B Hoijatie, "Thermal Incompatibility analysis of metal-ceramic systems based on flexural displacement data." ,*J Biomed Mater Res* vol. 41 ,pp. 614-623, 1998

2. ISO 9693 Metal Ceramic Dental Restorative Systems, 1999

3. Lenz J, S Schwarz, H Schwickerath, F Sperner, A Schaefer, "Bond strength of metal-ceramic systems in three-point flexure bond test", *J Appl Biomater* vol. 6, pp. 55-64, 1995

4. DeHoff P H, K J Anusavice, "Viscoelastic stress analysis of thermally compatible and incompatible metal-ceramic systems",*Dent Mater* vol. 14, pp. 237-245, 1998

5. Xin H, Y Li, X Ma, F Xu, W Guo, "The Investigation of Residual Stress Effect on Metal-ceramic Bond.",*Key Engineering Materials* vol. 274, pp. 1065-1070, 2004

6. Paul H. DeHoff, K J Ausavice, "Creep functions of dental ceramics measured in a beam-bending viscometer.", *Dent Mater* vol.20, pp. 297-304, 2004

7. DeHoff P H, K J Anusavice, "Shear stress relaxation of dental ceramics determined from creep behavior.", *Dent Mater* vol.20, pp. 717-725, 2004

8. Lenz J, S Kessel, "Thermal stresses in metal-ceramic specimens for the ISO crack initiation test (three-point flexure bond test)" ,*Dent Mater* vol.14, pp. 277-280, 1998

9. DeHoff P H, K J Anusavice, N Goetzen, "Viscoelastic finite element analysis of an all-ceramic fixed partial denture.", *J Biomech* vol.39(1), pp. 40-48, 2005

10. Timosehnko S, "Analysis of bimetal thermostats.", *J Opt Soc Am* vol.11, pp. 233, 1925

11. Schwarz S, J Lenz , H Schwickerath, "A contribution to the strength of the metal-ceramic bond in a flexure test.", *Dtsch. Zahnärztl.* Z.43:1, pp. 1152-1158, 1980

12. Griggs J A, M Yoda, T Konno, T Okabe, "Failure Analysis of Bonding of Binary Titanium Alloys to Porcelain.", *http://www.tambcd.edu/biomaterials/Posters/Griggs_AADR00.pdf*

13. ABAQUS/Standard manuals, version 6.5

14. Williams M L, R F Landel, J D Ferry, "Temperature dependence of relaxation mechanisms in amorphous polymers and other glass forming liquids.", *J. Am. Chem. Soc.* 77, 3701 3706, 1995